# Development of a Computer Vision and Deep Learning-Based Methodology for Fluid Interface Detection in Visual Separators for SCAL Experiments

*Diogo* Silveira[1,*], *Caio* Souza[1], *João* Abrantes[1], *Cláudia* Sheid[2], *Luís* Calçada[2], *André* Compan[3], *Luiz* Meleiro[2], and *Filipe* Furtado[2]

[1]Laboratório de Escoamento de Fluidos Giulio Massarani, R. UJ UFRRJ, Seropédica, Brasil
[2]Departamento de Engenharia Química, Universidade Federal Rural do Rio de Janeiro, UFRRJ, Seropédica, Brasil
[3]Centro de Pesquisa, Desenvolvimento e Inovação Leopoldo Américo Miguez de Mello, Petrobras S.A., Rio de Janeiro, Brasil

**Abstract.** The accuracy of the experimental data is crucial to the results obtained in Special Core Analysis (SCAL), particularly in relative-permeability experiments. The precise quantification of the produced fluids is used to calculate fluid saturations, as measurement errors propagate directly into the resulting relative-permeability curves and reservoir production forecasts. Various methodologies are used to quantify production in SCAL experiments, including ultrasonic and visual detection of the fluid's menisci. While manual or semi-automated reading and identification methods are already used in industry, they are prone to human subjectivity and parallax error, which can lead to low accuracy. Therefore, this work proposes a fully automated, high-resolution, and robust methodology for tracking fluid interfaces in visual separators. The proposed system integrates Deep Learning for meniscus detection with a computer vision framework that manages: (i) automated camera positioning to track interface displacement; (ii) Optical Character Recognition (OCR) and pattern recognition for high-resolution instrument reading; and (iii) optical distortion corrections. A high-precision measurement system was developed to replace the conventional human reading ruler-based method typically used in the SCAL experiment, thereby significantly reducing measurement uncertainty. Results demonstrate a more than one-order-of-magnitude increase in the precision of interface height measurements. The correlation between camera resolution and measurement sensitivity is also analyzed.

## 1 Introduction

The detection, measurement, and identification of liquid levels are essential tasks in industrial production, new product development, laboratory activities, and process control. Fluid level measurement techniques can also be applied to detecting menisci, which represent interfaces between two fluids and may occur in various systems. Menisci can form, for example, in conduits where immiscible fluids flow. One device designed for meniscus analysis is the visual separator used in relative permeability experiments.

Several experimental procedures belong to the field of petrophysics; among them, relative permeability testing is one of the most complex and important. In this test, under predefined experimental conditions, water and oil are simultaneously flowed through reservoir rock samples. This process produces a visible brine oil meniscus in the visual separator installed downstream of the rock sample. The internal dimensions of this device are known, and a graduated scale is attached to its front face. Images of the meniscus are captured with a digital camera, and the meniscus height relative to the scale is determined. These data are used to calculate flow rates, saturations, and relative permeability curves [1]. The precision of data obtained from relative permeability experiments directly affects predictions of recoverable hydrocarbon volumes, which in turn impact reservoir evaluation and company revenues.

Currently, when using visual separators in SCAL experiments, the oil and gas industry relies on manual verification of the captured images. An operator controls the camera during the experiment and later reads the meniscus height from each image. Because a single test may generate thousands of images, the procedure becomes repetitive and strongly dependent on operator experience. Consequently, automation and improved measurement accuracy are necessary to enhance the reliability of reservoir productivity estimations. Numerous studies have reported advances in fluid level detection techniques [2-5].

However, monitoring systems for menisci, like those observed in visual separators, have not been reported in the literature. Developing a robust solution requires consideration of several constraints. The visual separator has a narrow observation window, and the fluid tube is protected by a thick borosilicate (or sapphire) layer designed to withstand pressures of up to 10,000 psi. Because the system remains pressurized during testing, mechanical level-detection methods that require direct

* Corresponding author: diogosilveira@ufrrj.br

contact with the fluid are not feasible [5]. In addition, the level variations in the visual separator during the experiment generate pressure differences that are too small to be resolved with sufficient accuracy for reliable correlation between pressure measurements and liquid level. Consequently, pressure-difference-based sensors become impractical for this application [4, 6]

Relative permeability experiments also require strict temperature control of the equipment and fluids. For this reason, the entire experimental setup is placed inside an oven equipped with temperature control capability. Because the apparatus is enclosed and the oven reaches high temperatures (up to around 110 °C), detection methods based on ultrasonic techniques or capacitive sensors may be unsuitable for meniscus detection in the visual separator [7]

Liquid level measurement via meniscus analysis has been explored only to a limited extent, using a conventional scale attached to the visual separator and correcting for parallax and lens aberrations [8]. Another approach estimates oil content by analyzing light accumulation in images using edge-detection techniques [9]; however, this method does not support real-time image processing, unlike techniques used for monitoring levels in rivers and large reservoirs [10, 11].

Artificial intelligence approaches have also been proposed to verify liquid filling in bottles [12] or detect the presence of liquids [13]. Still, these solutions do not provide the precision required for visual separator applications, which must be at least ±0.5 mm. More recently, image-processing methods based on feature detection have been proposed for evaluating menisci and measuring liquid volumes [14]. Meniscus analysis has also been explored in laboratory settings to determine physical properties such as viscosity and density [2, 15]. Nevertheless, relative permeability experiments impose stricter constraints for menisci detection and analysis than those reported in these studies.

We present a methodology for real-time detection, monitoring, and analysis of menisci in visual separators used in core flooding experiments. The proposed methodology employs image processing and detection techniques for the preliminary processing of captured images and combines OCR models and deep learning algorithms for object detection and image mapping.

Additionally, a custom-built measurement scale (special ruler) was designed and installed alongside the visual separator. This scale incorporates specific visual symbols designed to facilitate detection by the artificial intelligence algorithm. It enables precise localization of the meniscus within the image. After detecting the meniscus and identifying the relevant objects in the image, corrections for parallax and lens aberrations are applied. The processed data are transmitted in real time to the control system, which automatically adjusts the camera position and records the measurements in a data logging system.

The use of visual separators introduces additional challenges, including the distance between the camera and the equipment, significant displacement of the meniscus relative to the measurement scale, different materials protecting the observation window, visual similarities between some immiscible fluids used in the experiment, and the high precision needed, all of which are taken into account in the scope of this study.

The reading is performed automatically and uses our developed ruler, for which the maximum achievable precision depends on the resolution of the captured images and, thus, on the camera used during the fluid's volumetric measurements. In the experiments conducted in this study, the images have a vertical resolution of 480 pixels. Given that in our experiment, 4 cm corresponds to 480 pixels, an approximate measurement resolution of 0.083 mm per pixel can be obtained. The achievable precision is approximately six times higher than that of human readings with a standard ruler (±0.5 mm) when the operator's performance is flawless (i.e., no errors).

## 2 Materials and Methods

The materials and methods section is organized into descriptions of the experimental apparatus, the methodology for the computer vision algorithm developed for meniscus detection and evaluation, and the data analysis methods used in this study.

### 2.1 Experimental Apparatus

The experimental apparatus used during this study consists of a visual separator, a high-precision pump, an automated displacement system coupled with a camera, an illumination system, and a control unit. Figure 1 shows part of the system, including the visual separator, camera, step motor, illumination system (two 20-watt white LED lamps), and the endless screw on which the camera can move.

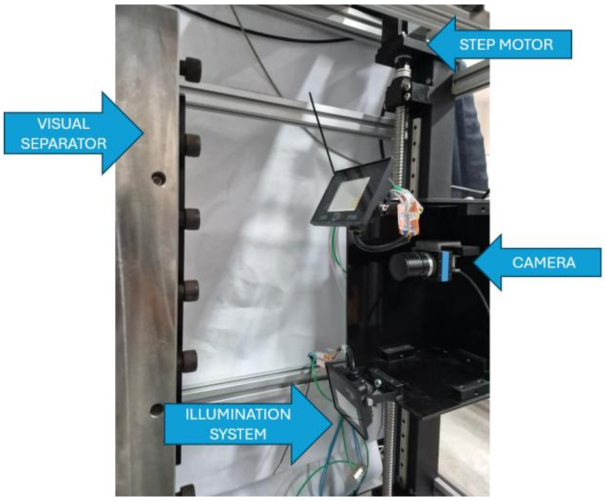


**Fig 1.** Part of the experimental apparatus consists of a visual separator, a camera, an illumination system, and a step motor.

The camera used on the prototype is a DMK 22AUC03 from IMAGING SOURCE with a 16-millimeter lens. Each image acquired by the camera has a resolution of 744×480 pixels and is monochromatic. The automated system uses a 24 kgf step motor with a control driver.

Communication, image acquisition, and displacement controls were implemented using the CDAQ-9179 and the appropriate cards obtained from National Instruments, along with a LabVIEW program built on the actor's framework (an object-oriented architecture of independent actors that communicate through asynchronous messages while running in parallel). An Ametek Chandler Engineering pump, model Quizix QX-20K (accuracy of ±0,1% on the set flow rate), is also controlled by our system.

The LabVIEW 2026 software, Pumpworks software (pump control), and scripts for deep learning training were installed on a computer with a 13th-generation Intel Core (i7-13700), 32 GB of RAM, a 12 GB RTX 3060 video card, and 1 TB of disk space (SSD).

Figure 2 presents the visual separator used in the experiment. It is a custom-made piece of equipment with a narrow window of borosilicate glass resistant to pressures up to 10,000 psi. Inside the equipment, a channel with a precise volume of 30 milliliters is machined, establishing a correlation between the ruler and the visual separator at 1 centimeter to 1 milliliter.

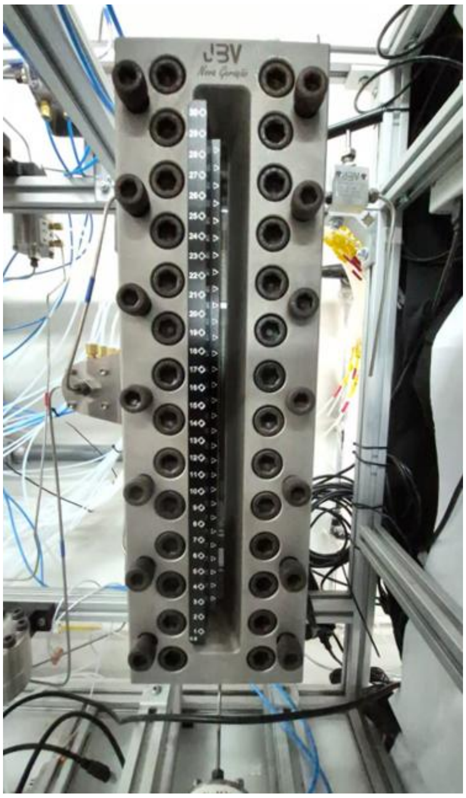

**Fig 2.** Visual separator coupled with a custom-made ruler.

In addition to the visual separator shown in Figure 2, a new type of ruler was implemented for this experiment. Instead of having the usual ticks, this ruler is composed of two figures, rotated squares and triangles, equally spaced (1 cm in the vertical direction) on the two reading areas, and their corresponding numbers are also engraved on the ruler. Along with this new implementation, a black-and-white ruler was chosen to facilitate easier detection and image processing in the vision detection algorithm.

## 2.2 Methodology

A new methodology was developed for this experiment, with the primary objective of improving the precision of each meniscus reading used in advanced core-flooding experiments.

The proposed methodology, schematized on Figure 3, consists of seven main steps: 1) image acquisition and correction; 2) reading the numbers on the ruler; 3) identification of symbols and their location; 4) inference using a neural network for menisci detection; 5) correlation for all information acquired and translation to pixel-position on image; 6) optical correction of menisci position; and 7) final step to deliver the correct reading and send the information to a logger system.

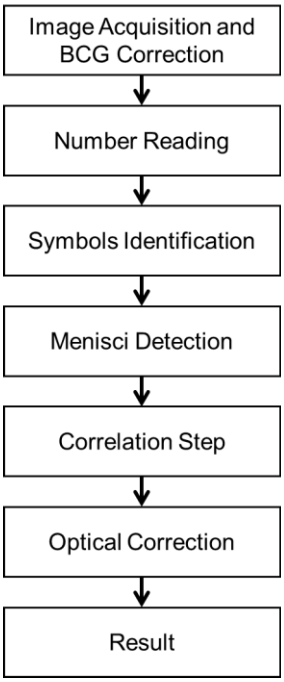


**Fig 3.** Flowchart of the steps for the proposed methodology.

When an image of the visual separator is acquired using the developed program, the proposed methodology is triggered to report the meniscus height on the equipment. In the first step, after image acquisition, Brightness, Contrast, and Gamma (BCG) correction is applied; all parameters for this correction must be determined in advance based on the experimental apparatus and the local illumination in which the experiment is conducted. These initial parameter settings are determined empirically before the experiment to avoid overexposure (high brightness) or underexposure (dark image) in the acquired frame.

The number-reading step is performed by defining a Region of Interest (ROI), a delimited area in the image where the search algorithm can be applied. Before the methodology applies the Optical Character Recognition (OCR) algorithm to extract numbers from the image, a binarization process is applied to the ROI, converting the extracted portion of the image to black and white. Figure 4 shows the standard result of this process, which is the bounding box positions and values for each recognized character.

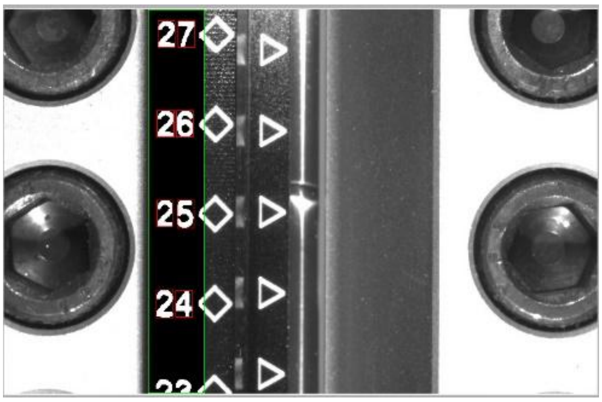


**Fig 4.** Standard results of ROI binarization and OCR analysis.

After this step in the methodology, the system starts the symbol identification. As in the number identification step, a ROI is determined, and LabVIEW's pattern search algorithm identifies all squares and triangles in the image, returning their center positions and bounding boxes.

Menisci are detected using an inference algorithm based on the convolutional neural network Yolo V8 [16], trained on a dataset of meniscal images under multiple illumination conditions across the length of the visual separator.

After an inference of the menisci's position, a ROI 20% bigger in relation to the menisci's bounding box is placed around its central origin point. Using the new ROI area, a cropped image is extracted from the main image, and binarization and morphological operations are applied to the meniscus-cropped image.

Based on the processed, extracted image, the pre-tuned LabVIEW edge-detection tool is applied to each vertical line of pixels. This tool returns the pixel position of the edge based on a gradient computed from differences in the image's pixel intensities.

All data relevant to the artifacts in the image, their positions relative to the image, and their absolute values, acquired during the first four parts of the methodology, are saved in the system. Figure 5 shows an example of these results, which are an overlay of numbers and symbols with their bounding boxes, with a point indicating the meniscus position.

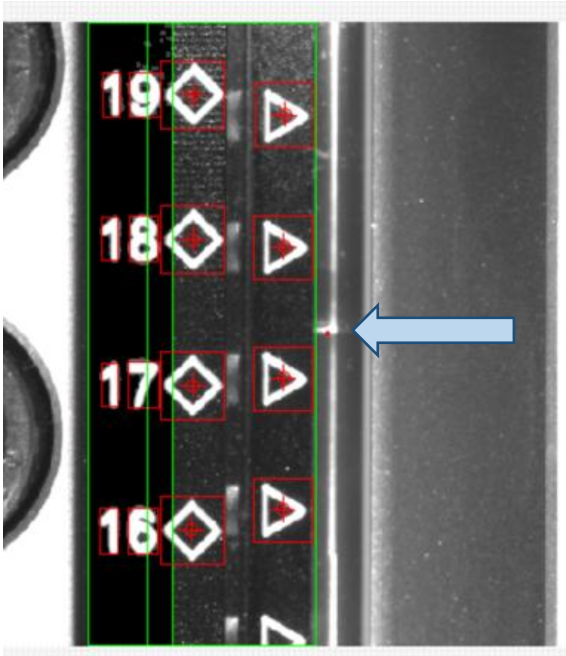


**Fig 5.** Overlay of data acquired during the first four steps of the proposed methodology (arrow points the detected meniscus).

All data from numbers, symbols, and menisci are compiled into a single matrix to correlate each read number with a specific square and triangle position, as well as the position of the best edge in each frame. The next step in the methodology is the optical correction of the acquired position for each artifact (menisci, squares, triangles, and number values).

Using the best edge position identified in the image, the control system moves the camera to keep the meniscus centered in the frame, where aberration errors are smaller. For smooth camera movement and automatic control of the camera independent of the meniscus' velocity, a PID control algorithm was implemented. This constraint is used as a reference for the optical correction of the menisci's position.

Figure 6 shows a schematic of optical correction using our custom-made experimental apparatus. Based on the visual separator project, the distance between the faces of each ruler, the thickness of the borosilicate, and any other physical distance are known. Together, the supplier informed the refractive index for the borosilicate glass. The distance $L_{r1}$ is known (position of the menisci in the image), and $L^*$ is the meniscus's true position, obtained after the correction.

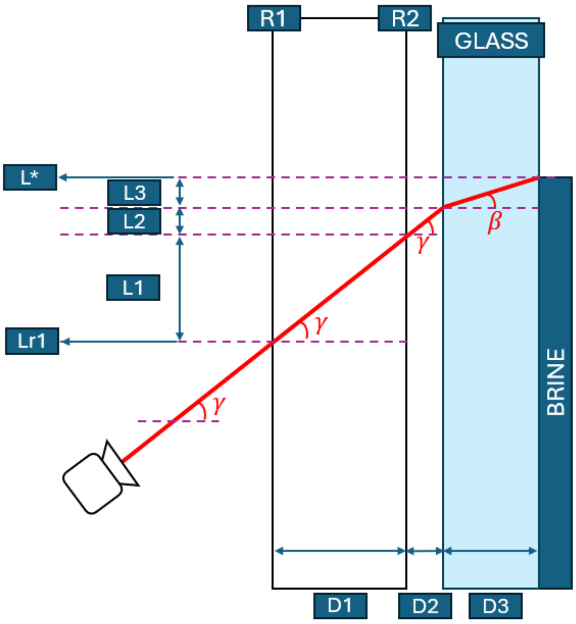


**Fig 5.** Scheme for optical correction and trigonometry analysis.

All position relations derived from the image are pixel-based and require a conversion between centimeters and pixels. As a result, a calibration process was performed. The methodology requires calibration before the first experiment or if any physical modification is made to the apparatus. The calibration consists of setting the camera position at seven equally spaced, known values along the ruler. Using these seven ruler values and the square and triangle positions, a linear adjustment is applied to the centimeter-pixel correlation for each ruler.

For each set of values acquired during calibration, the difference between the square and triangle positions is calculated using a centimeter-to-pixel correlation and divided by the distance between ruler 1 and ruler 2. The tangent of this value is the gamma angle of the experiment.

The menisci are located behind a borosilicate layer. According to Snell's law, refraction at this layer produces a new light propagation angle, as described by Equation 1.

$$n_1 \sin\gamma = n_2 \sin\beta \quad (1).$$

The real position of the menisci ($L^*$) is given by Equation 2.

$$L^* = L_{r1} + L_1 + L_2 + L_3 \quad (2).$$

Using trigonometry relations, Equation 1 and Equation 2, the difference between the read value on the image and the real position ($\Delta L$) is obtained by Equation 3,

$$\Delta L = (\mathrm{D}_1 + \mathrm{D}_2)\tan(\gamma) + \mathrm{D}_3 \tan\left[\arcsin\left(\frac{\mathrm{n}_1 \sin(\gamma)}{\mathrm{n}_2}\right)\right] (3),$$

where $D_1$, $D_2$, and $D_3$ are known dimensions of the visual separator.

As the final step in the methodology, the system reports the results via a human-machine interface and a logging algorithm that saves all data to a spreadsheet. The proposed methodology is applied to every frame requested by the system and is based on an imposed time loop.

For results analysis and validation, the AARD% (Average Absolute Relative Deviation), shown in Equation (4) was utilized.

The AARD% evaluates the absolute relative deviation for two datasets. In this work, the datasets consist of the volume variation over time measured by our developed system ($V_{model}$) and the volume displaced by the precision pump ($V_{pump}$), which is considered the reference (our ground truth).

$$AARD\% = \frac{100}{n}\sum_{i=1}^{n}\left|\frac{V_{model,i} - V_{pump,i}}{V_{pump,i}}\right| \quad (4).$$

## 3 Results and Discussion

This study performed twelve experiments to evaluate the experimental apparatus and the proposed methodology. The information about the test is shown in Table 1, which includes the experiment label, the pump flow rate (in milliliters per minute), the experiment duration, and the sampling rate used during data post-processing. The setup achieved a processing time of less than 500 milliseconds per loop, including the entire operation.

The experiments were performed under the same conditions within the experimental apparatus, using brine and light mineral oil in the visual separator to induce meniscus formation. Both liquids are translucent, form a thin interface with no emulsion, and exhibit low contrast. These characteristics are a challenging scenario and have direct implications for the software detection and methodology, justifying the adjustment of the illumination parameters before the experiment. It is important to note that working with petroleum-brine or petroleum-gas would make detecting the interface easier, since the contrast between them is more pronounced than between two translucent liquids. However, menisci formation may be affected by various conditions (higher temperatures and pressures, severe use of the visual separator, emulsion formation in the interface), resulting in distorted menisci that are outside the scope of this study but can be analyzed using our methodology, thereby adding new training data to the deep learning model.

The experiments were conducted at atmospheric pressure and room temperature (approximately 22°C). The signal on pump rates indicates the direction of the fluid flow. Positive values indicate fluid is being added to the visual separator; negative values indicate the pump is removing fluid.

**Table 1.** Experiment information.

| Experiment | Pump rate (mL/min) | Duration | Sampling rate |
|---|---|---|---|
| 1 | -5.000 | 00:03:00 | 1s |
| 2 | -4.000 | 00:03:30 | 1s |

| | | | |
|---|---|---|---|
| 3 | -3.000 | 00:04:45 | 1s |
| 4 | -2.000 | 00:07:30 | 10s |
| 5 | -1.000 | 00:15:00 | 10s |
| 6 | 0.500 | 00:29:56 | 30s |
| 7 | -0.100 | 02:29:53 | 1min |
| 8 | 0.100 | 02:29:49 | 1min |
| 9 | -0.050 | 00:41:38 | 30s |
| 10 | -0.050 | 04:59:15 | 5min |
| 11 | -0.010 | 04:56:00 | 10min |
| 12 | -0.005 | 07:37:55 | 20min |

Due to the resolution constraints of our experiment, any measurements of the visual separator with changes smaller than 0.083 mm are beyond the apparatus's resolution. Therefore, only 3 significant figures were used in data acquisition, and 2 in any subsequent calculations for data in mm. The use of the correct figures implies that less noise is applied to the accumulated sum, and the error is expected to be smaller due to the removal of the numerical noise.

The AARD% was calculated for each experiment using the accumulated volume values reported by our system and the pump, applying the methodology. In all experiments, the ground truth used for comparison and analysis is the reported volume given by the pump. Table 2 shows the AARD% and the slope of the linear adjustments between time and accumulated volume ($V = at$) for each experiment. The slope for the $V = at$ gives the flow rate.

We used the reported values in the pump software as the reference values for comparison with the methodology results, given the pump's high precision and accuracy.

It is important to note that we have measured the average error introduced by the pump through independent experiments that measure and weigh the volume of pumped fluid over a given time. Using the fluid density and the mass collected over time, we calculated the total pumped volume and volumetric flow rate, which showed errors of up to 1.0% relative to the values reported by the pump software.

**Table 2.** Experimental Average Absolute Relative Deviation (AARD%), slope for the linear relation between accumulated fluid volume and time ($V = at$, where $a$ is the volumetric flow rate) obtained by our measurement system, and that calculated using the data reported by the pump software.

| Experiment | AARD% | Methodology Slope (mL/min) | Pump Slope (mL/min) |
|---|---|---|---|
| 1 | 3.21 | 5.13078 | 4.99853 |
| 2 | 2.71 | 4.09655 | 3.99925 |
| 3 | 1.95 | 3.04944 | 2.99982 |
| 4 | 3.32 | 2.00252 | 1.99957 |
| 5 | 2.64 | 1.00432 | 1.00000 |
| 6 | 2.05 | 0.50644 | 0.49994 |
| 7 | 2.68 | 0.10260 | 0.09998 |
| 8 | 1.06 | 0.10026 | 0.09997 |
| 9 | 2.85 | 0.05067 | 0.04999 |
| 10 | 5.01 | 0.04997 | 0.05000 |
| 11 | 2.64 | 0.01029 | 0.01000 |
| 12 | 5.69 | 0.00516 | 0.00500 |

The slopes showed a good agreement between our system and the considered ground truth (pump data reported in its software), showing deviations ranging from -0.06 to 3.20%.

Figures 6, 7, 8, and 9 show an example of data acquisition using the methodology, with software-reported pump volumes plotted together with our system-reported volumes at various pump-imposed flow rates. For clarity, all plotted data were normalized to represent the total volume displaced, regardless of displacement direction. The coefficients in Table 2 were calculated based on this data.

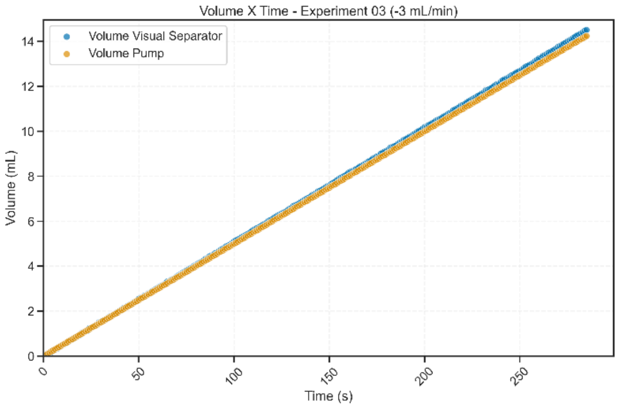


**Fig 6.** Relationship between measured volumes on the visual separator and the software-reported pumped volume at a flow rate of 3 mL/min over time. Obtained from experiment 03.

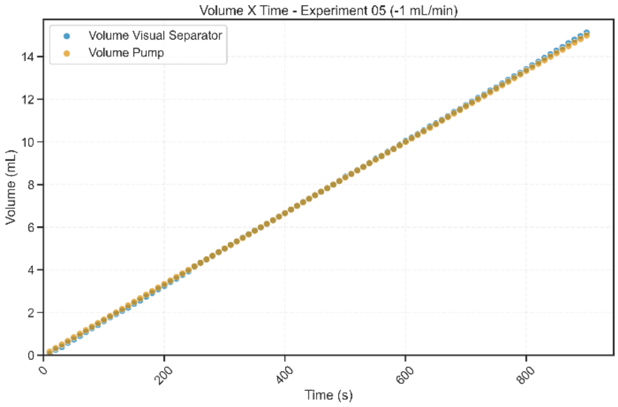


**Fig 7.** Relationship between measured volumes on the visual separator and the software-reported pumped volume at a flow rate of 1 mL/min over time. Obtained from experiment 05.

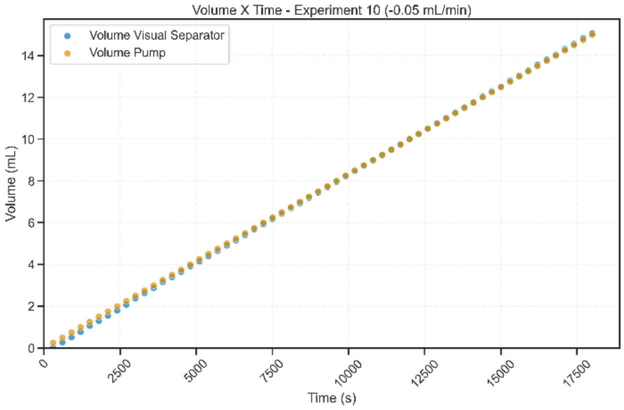


**Fig 8.** Relationship between measured volumes on the visual separator and the software-reported pumped volume at a flow rate of 0.050 mL/min over time. Obtained from experiment 10.

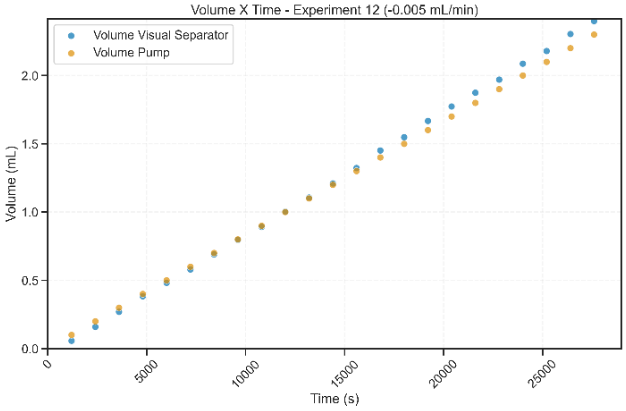


**Fig 9.** Relationship between measured volumes on the visual separator and the software-reported pumped volume at a flow rate of 0.005 mL/min over time. Obtained from experiment 12.

The comparison between the two data series shown in Figures 6, 7, 8, and 9 suggests a strong correlation between the pump-displaced volumes and the volumes measured with our system.

The total duration of each experiment varied because higher flow rates caused the menisci to move faster through the visual separator. Nevertheless, a deviation is noticed in some cases, particularly at the beginning or near the end of the experiment. This deviation is due mainly to two sources, which are: (1) the change between the considered best edge for meniscus position detection, for example, from the bottom to the upper edge as it moves through the visual separator; and (2) the low camera resolution, which gives a poorer resolution when compared to high-end cameras.

The developed system has a high sampling rate for image acquisition and frame analysis. During the experiments, each frame's acquisition and complete analysis, which resulted in a meniscus reading, took approximately 300 milliseconds.

Observations of the collected data showed that a high number of acquired frames may introduce noise into the meniscus reading over time. As a result, during post-processing, several data points were excluded based on their time intervals. The minimum time interval was set to 1 second.

Therefore, the data used for all analyses, including the results shown in Table 2, were sampled into a new data frame before applying the post-processing step based on the sample times shown in Table 1.

To compare the accuracy of our system, we have plotted (Figures 10, 11, 12, and 13) the 45° expected curves between the ruler-based volume measurements made by our system and the reference data (the displaced volume reported by the pump software). We also show in these Figures the ideal curve (45° slope) and the respective curves for ±5% deviations.

The results from ruler readings taken by our system showed good agreement with the reference values. The observed maximum deviation between our ruler readings and the pump readings was no more than 6% at the lower flow rate (0.005 mL/min). At this flow rate, fluid displacement in the visual separator is slow, and the sampling rate used for this case (20 min, or 1200 s) is expected to cause a displacement of 0.100 mL, corresponding to 1 mm of travel in the visual separator.

For the total duration of experiment 12, only 22 usable data points were obtained for analysis, which makes the data more prone to punctual error. If the sampling rate were set to 2 min, we would expect a displacement of 0.1 mm, which is close to our method's resolution (±0.083 mm/pixel, approximately 0.1 mm/pixel), leading to an uncertainty of approximately ±100% for the first data points.

Therefore, for smaller flow rates, it is necessary to have a longer sampling time and longer experiments to have a good detection of the meniscus movement with a small uncertainty. These results point to the need for a higher-resolution camera to achieve smaller uncertainty and are consistent with the second statement above, which explains the sources of deviations between our readings and the pump readings.

Additionally, we can analyze two sets of experiments that used the same flow rates, which are the 7-8 (0.1mL/min, with nearly the same acquisition time) and 9-10 (0.05mL/min, with different acquisition times) pairs. While increasing the experiment time for the 9-10 pair reduced the deviation from the ground truth from 1.36% to 0.06%, maintaining the same acquisition time for the 7-8 pair resulted in deviations of 2.62% and 0.29%, respectively. These results indicate that both statements above hold, with deviations arising from changes in the choice of the meniscus's best edge during the experiment (*e.g.*, bottom-to-top) and from the need for higher resolution, especially at the lower flow rates.

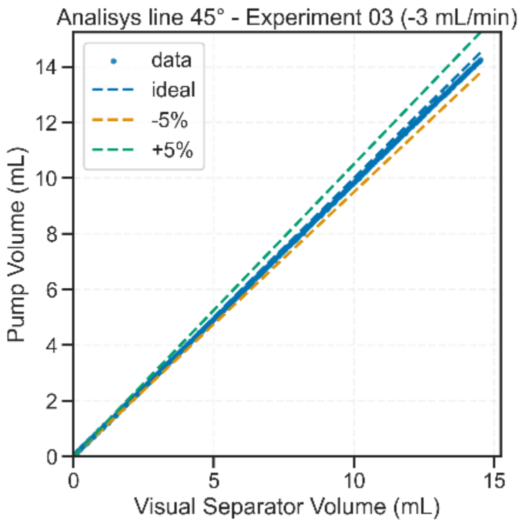


**Fig 10.** Relationship between measured volumes on the visual separator and the pump for a flow rate of 3 mL/min.

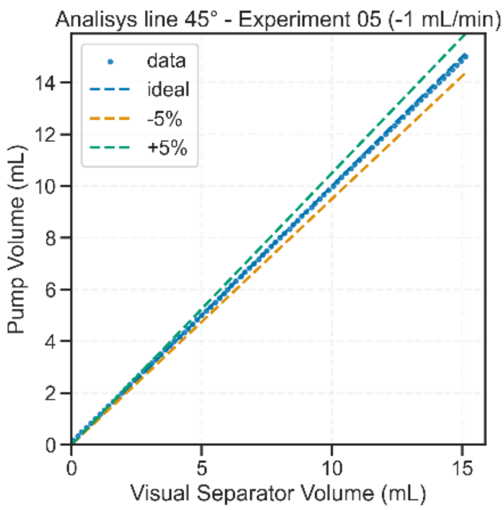


**Fig 11.** Relationship between measured volumes on the visual separator and the pump for a flow rate of 1 mL/min.

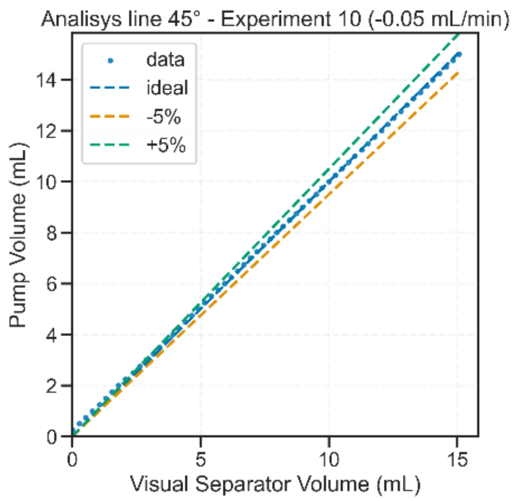


**Fig 12.** Relationship between measured volumes on the visual separator and the pump for a flow rate of 0.05 mL/min.

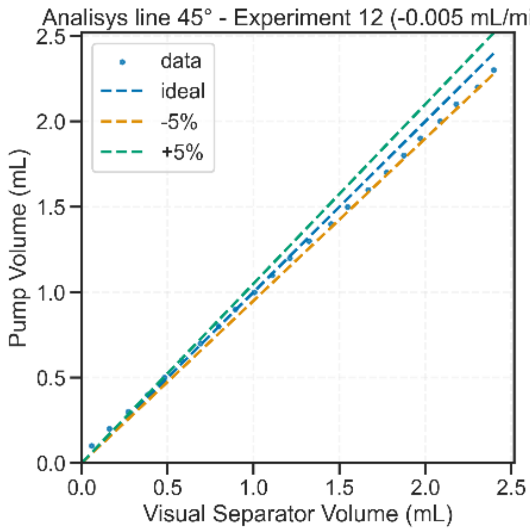


**Fig 13.** Relationship between measured volumes on the visual separator and the pump for a flow rate of 0.005 mL/min.

Precision is a key concern in developing the proposed methodology because it directly affects the dependency of the relative permeability curves on the fluid's saturation within the core [17]. Thus, introducing additional uncertainties in fluid's saturation determination would cause even greater uncertainties in relative permeability curves than those reported in the literature [17].

An operator reading the images acquired during the relative permeability experiment has only a one-millimeter resolution. To compare our methodology with a human reading the ruler, we make the following assumptions: (a) the operator makes a perfect reading within the ruler's resolution, which is 1 mm; (b) the operator corrects all parallax and lens effects perfectly, which means no parallax and lens aberrations are plaguing their readings; and (c) the maximum error the operator input in the readings is the measurement of one reading only, which means the maximum absolute uncertainty is fixed to the ruler's uncertainty. Given our assumptions, the maximum expected deviation among operators would be ±1 mm throughout the experiment. In Figures 14 to 17, we show the evolution of percent error as a function of displaced volume relative to the ground truth for our system and the perfect human reading as stated above.

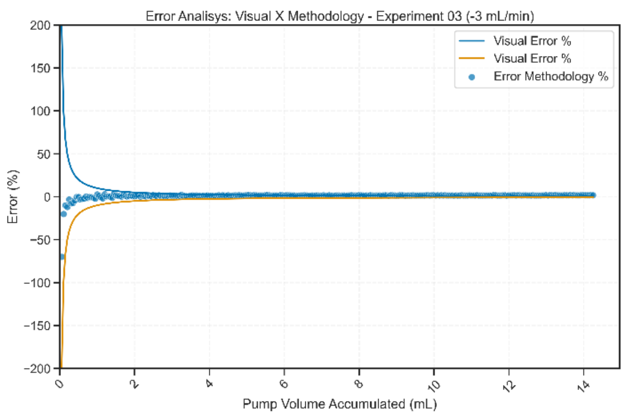


**Fig 14.** Comparison between the proposed methodology error and a perfect visual reading error (±1 mm maximum between

different operators) with displaced volume for a flow rate of 3 mL/min.

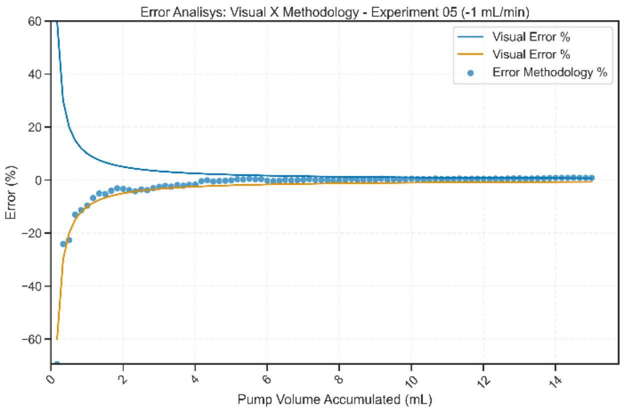


**Fig 15.** Comparison between the proposed methodology error and a perfect visual reading error (±1 mm maximum between different operators) with displaced volume for a flow rate of 1 mL/min.

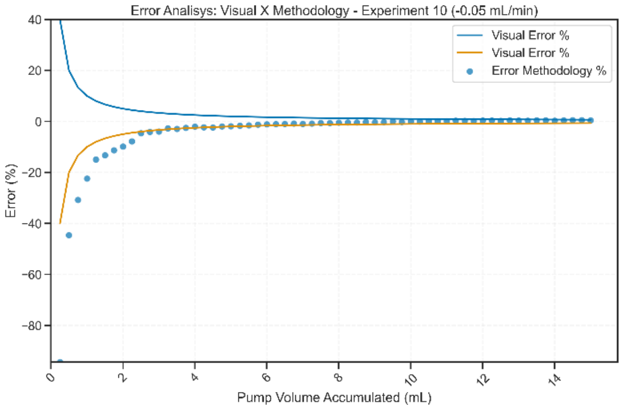


**Fig 16.** Comparison between the proposed methodology error and a perfect visual reading error (±1 mm maximum between different operators) with displaced volume for a flow rate of 0.05 mL/min.

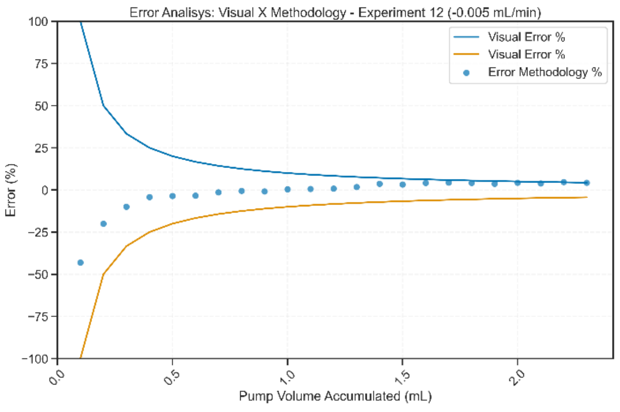


**Fig 17.** Comparison between the proposed methodology error and a perfect visual reading error (±1 mm maximum between different operators) with displaced volume for a flow rate of 0.005 mL/min.

Our system yields measurements with smaller average errors than a perfect human reading in all cases except 2 (4 and 10), which are addressed in the next paragraph. However, it is possible to observe fluctuations in the data shown in Figures 14-17. These fluctuations can be reduced by addressing the two statements given earlier in this chapter, such as using a higher-resolution camera and averaging the best edges from the menisci obtained by gradient analysis using both directions: from bottom to top and from top to bottom. Table 3 shows the average error comparison for each experiment between our methodology and the perfect human reading.

**Table 3.** Average Absolute Relative Error comparison for each experiment between our methodology and the perfect human reading.

| Experiment | AARD% Proposed methodology | AARD% Perfect human reading |
|---|---|---|
| 1 | 3.21 | 3.88 |
| 2 | 2.71 | 4.23 |
| 3 | 1.95 | 4.37 |
| 4 | 3.32 | 2.93 |
| 5 | 2.64 | 3.39 |
| 6 | 2.05 | 3.16 |
| 7 | 2.68 | 3.75 |
| 8 | 1.06 | 3.75 |
| 9 | 2.85 | 24.11 |
| 10 | 5.01 | 3.12 |
| 11 | 2.64 | 13.66 |
| 12 | 5.69 | 16.24 |

Since displaced volume is proportional to time through the flow rate, a larger volume displaced at the same flow rate indicates a longer experiment. Because of the characteristics of an automated system, the relative error reaches a steady state after a certain time, unlike the perfect visual reading as considered in this work, where the error tends to zero over time. This is evident in cases 4 and 9-12. While in cases 4 and 10 the time was sufficient to diminish the error, that was not the case for experiments 9, 11, and 12, which showed larger errors.

# 4 Conclusion

Fluid-level analysis and meniscus displacement detection are important for special core analysis, particularly in relative permeability experiments using visual separators. Data precision is related to oil reservoir production and financial viability analysis. Although the literature contains numerous studies on liquid level detection, most focus on optical corrections, laboratory-scale analysis, or applications where high precision is not critical. Thus, a notable scarcity of studies addressing the visual separator and methodological improvements remains. It is also noted that the accuracy achieved in core-flooding experiments is proportional to the volume of fluid displaced.

In this study, the proposed methodology yielded results with precision and repeatability suitable for experimental core-flooding analysis. The error analysis also demonstrates the apparatus's ability to reduce operator dependence on visual reading while improving the data quality, accuracy, consistency, and precision of the results. Automation capability is also achieved through this methodology; however, using our proposition requires specialized equipment and artificial intelligence tools.

The results demonstrate a strong dependence on camera resolution and image quality, primarily because illumination conditions can affect meniscus edge detection, which together causes most of the reported errors/uncertainties in this paper. Additionally, higher precision at the beginning of experiments at low flow rates may not be achieved due to the maximum reading resolution. Moreover, because the core flooding experimental duration depends on the total fluid displacement, which is linked to the core sample's pore volume, accuracy increases with sample characteristics.

Within the scope of this study, the methodology proved effective, and future tests with a higher-resolution camera under high-pressure and high-temperature conditions are needed to assess the system's precision under reservoir-representative conditions.

## Acknowledgments

The authors would like to thank PETROBRAS (Petróleo Brasileiro S.A.) for funding and support, as well as UFRRJ and the Fluid Flow Laboratory for their support in the development of this work.

## References

1. C. McPhee, *Core analysis: A Best Practice Guide* (Elsevier, Volume **64,** 2015)
2. A. B. Hajeb, S. A. Shukor, C. S. Tan, Advancements in liquid level detection systems: A comprehensive review and novel approach, *IOP Conference Series: Earth and Environmental Science,* **1516** (2025)
3. P. Mohindru, Development of liquid level measurement technology: A review, *Flow Measurement and Instrumentation*, **89** (2023)
4. Y. Singh, S. K. Raghuwanshi, S. Kumar, Review on Liquid-level Measurement and Level Transmitter Using Conventional and Optical Techniques, *IETE Technical Review*, **36(4)** (2018)
5. B. Jin, X. Liu, Q. Bai, D. Wang, Y. Wang, Design and Implementation of an Intrinsically Safe Liquid-Level Sensor Using Coaxial Cable*, Sensors*, **15(6)** (2015)
6. A Jabiyeva and G Isgandarova, Devices for automatic control of the quantity and 3 quality of oil in tanks, *IOP Conference Series: Earth and Environmental Science*, **1254(1)** (2023)
7. R. Muñoz, J. Fuentealba, S. Michea, P. A. Santana, J. I. Martínez, N. Casanova-Morales, V. S. Barrera, Ultrasonic Sensor: A Fast and Non-Destructive System to Measure the Viscosity and Density of Molecular Fluids, *Biosensors*, **14(7)** (2024)
8. G. Bobovnik, T. Mušič, J. Kutin, Liquid Level Detection in Standard Capacity Measures with Machine Vision, *Sensors*, **21(8)** (2021)
9. Q. Liu, B. Chu, J. Peng, S. Tang, A Visual Measurement of Water Content of Crude Oil Based on Image Grayscale Accumulated Value Difference, *Sensors*, **19(13)** (2019)
10. G. Chen, K. Bai, Z. Lin, X. Liao, S. Liu, Z. Lin, Q. Zhang, X. Jia, Method on water level ruler reading recognition based on image processing, *Signal, Image and Video Processing*, **15(1)** (2020)
11. D. Zhang, J. Tong, Robust water level measurement method based on computer vision, *Journal of Hydrology*, **620** (2023)
12. J. Musić, I. Stančić, B. Džaja, V. Pekić, Image-Based Sensor for Liquid-Level Monitoring during Bottling, with Applications to Craft and Home Brewing, *Sensors*, **23(16)** (2023)
13. Y. Wu, H. Ye, Y. Yang, Z. Wang, S. Li, Liquid Content Detection In Transparent Containers: A Benchmark, *Sensors*, **23(15)** (2023)
14. W. Shao, Y. Wang, D. Wu, Q. Gao, M. Shokouhimehr, Z. Liu, A Method for Measuring Liquid Volume in Transparent Glass Vials Utilizing Image Processing and Feature Recognition, *IEEE Transactions on Instrumentation and Measurement*, **74** (2025)
15. R. Xing, B. Li, J. Chen, R. Liu, Small-Capacity Liquid Density Detection Device Based on Computer Vision, *8th International Conference on Advanced Algorithms and Control Engineering (ICAACE)*, (2025)
16. G. Jocher, A. Chaurasia, J. Qiu, Ultralytics YOLOv8, (2023), Available on Github repository: https://github.com/ultralytics/ultralytics
17. S. Berg, E. Unsal, H. Dijk, Non-uniqueness and uncertainty quantification of relative permeability measurements by inverse modelling, *Computers and Geotechnics*, **(132)** (2021)